

Proceedings of the ASME 2022 Heat Transfer Summer Conference HT2022 July 11-13, 2022, Philadelphia, Pennsylvania

HT2022-85681

IMPROVED FEMTOSECOND 3D LIGHT FIELD LITHOGRAPHY WITH A PHASE-CONTROLLED SPATIAL LIGHT MODULATOR

Aravind Jakkinapalli, Sy-Bor Wen*

TAMU, College Station, TX

ABSTRACT

Through years of development, we have successfully demonstrated 3D light field lithography with UV continuous light. We recently combined this approach with femtosecond laser sources as two-photon femtosecond 3D light lithography. It is found that consistent results can happen under limited conditions with this direct combination. Our theoretical analysis reported last year shows that the experimental difficulty can be attributed to digital micro-mirror devices (DMD) and microlens arrays (MLA) used in the current 3D light field projection. Though they can control the propagation directions and interact at designed 3D locations, rays from such a system diverge with respect to the propagation distance. As a result, 3D voxel intensity in the 3D projection changes as a function of the separation distance with respect to the MLA in the 3D projection. To solve this problem, we replace the combination of DMD and MLA with a phase-controlled spatial light modulator. With a labdeveloped algorithm, a single femtosecond laser pulse can generate up to a million sub-rays through the phase-controlled spatial light modulator. These sub-rays with a precisely controlled propagation direction can intersect at designed 3D locations as voxels for 3D virtual object constructions. Moreover, these sub-rays have minimum divergence angles to ensure that the voxel intensities are maintained consistently at each 3D location. We also demonstrated that versatile 3D patterns could be generated with two-photon femtosecond 3D light field lithography based on this innovative approach.

Keywords: femtosecond laser, microfabrication, 3D fabrication, 3D lithography, microscale optical energy transfer

1. INTRODUCTION

Following the demand for miniaturization of products in the recent decade, fabrication of 3D microstructures is becoming increasingly common due to a significant reduction in the weight to performance ratio compared to their 2D

counterparts. For example, 3D structures are adopted in newer generations of microelectromechanical devices[1, 2]. Most of the single bio cell culturing devices rely on 3D microsystems[3-6]. Also, microscale 3D scaffolds are required in 3D tissue bioprinting for tissue regeneration[3, 7]. Most of our current 3D microfabrication techniques are based on layer-by-layer stacking of 2D fabrications, also known as 2.5D microfabrication. This 2.5D microfabrication, such as stereolithography, though it can provide high spatial resolution[8], suffer from the requirement of supporting structs in the fabrication of complicated 3D structures[9]. Thus, there is a need for a proper 3D microfabrication technique capable of fabricating 3D structures with fewer geometry limitations.

Two-photon scanning lithography is a flexible technique of 3D fabrication with sub-micron resolution[10, 11]. However, it is a slow point-by-point approach process which makes it impossible to fabricate cm³ level structures. Holographic lithography is one method where 3D structures are directly patterned without the need for scanning or layer-by-layer stacking. However, the required coherent reference beam in holography can create unwanted speckles due to random interference, reducing the quality of the 3D holographic projection[12, 13]. Also, 3D holographic lithography is limited to only fabricating complex structures along the surface but not in the interior regions of the object.

To have a fast throughput 3D fabrication, we proposed a new methodology is based on 3D projection through a combination of DMD and MLA[14, 15]. Such technique is originally derived from the light field imaging concept in plenoptic cameras, where the direction and intensity of rays emanating from an object are recorded and displayed. Inversely, a virtual object can be projected and in a 3D space. Inspired by this logic, we developed a ray-tracing technique allowing us to generate voxels at arbitrary 3D locations through a combination of directional laser light, DMD, and MLA. We successfully projected voxel clouds to form different 3D geometries with continuous UV light and femtosecond light at visible wavelengths with such a method[14,

16]. Also, we successfully compressed these 3D voxel clouds to microscale with a telecentric lens pair for 3D microscale lithography. Since all the voxels are projected simultaneously, no point-by-point scanning is required as in previous laser-based 3D patterning.

During the demonstration of 3D lithography with 3D projections based on the combination of DMD and MLA, we observed increasing in voxel size as a function of the separation distance between the projected voxels and the MLA. Such an unwilling increase of the voxel size is because of the divergence of rays forming each voxel after passing through the MLA. The increase of voxel size and the associate decrease of light intensity of each voxel as a function of separation caused difficulty in curing photoresist uniformly at the 3D projection domain. To solve this difficulty, a new 3D volumetric projection method based phase-only spatial light modulator is developed in this study. Using the capability of controlling the wavefront of redirected rays, we are able to manipulate millions of rays propagating at designed directions without divergence. Voxels generated from these nearly nondivergent micro rays can have consistent intensity and size at all the 3D positions. Algorithms of using phase-only spatial light modular to form voxels in 3D spaces as well as the preliminary tests of femtosecond microscale 3D lithography with this novel 3D volumetric projection are presented in the following sections.

2. EXPERIMENTAL PROCEDURE

2.1 Setup

A 3D light field based lithography system was previously developed by us to generate 100s of micrometers scale patterns using a 520 nm femtosecond laser source[14, 16]. The system is illustrated in figure 1. The Digital Micrometer Device (DMD) was selected as the Spatial Light Modulator (SLM) to control the on/off state of each individual light beam, and the MLA controlled the direction and angles of the light beams. By coupling the DMD with the MLA, we could generate voxels at required 3D positions to create 3D geometries like walls and wedges, as shown in figure 2a. This technique could project 3D structures, but the intensity at the voxel location varied as a function of the distance between the voxel and the MLA plane. This variation is a consequence of the convergent/divergent behavior of the light beam from each DMD pixel. The parallel light beam sent from the DMD converges and begins diverging at the 1f plane of the MLA. The voxels formed at locations closer to the 1f plane by n rays are smaller and have a more localized intensity distribution compared to the voxels formed at a farther location, as illustrated in figure 2b. To prevent this intensity variation between the voxels, we observed the need to retain the direction control functionality of the MLA without inducing the unwanted hassle of converging and diverging the beam before the voxel location. The DMD is an amplitude control device and hence cannot manipulate the direction of the incoming light. We propose using a phase-controlled SLM to replace the DMD and the MLA combination.

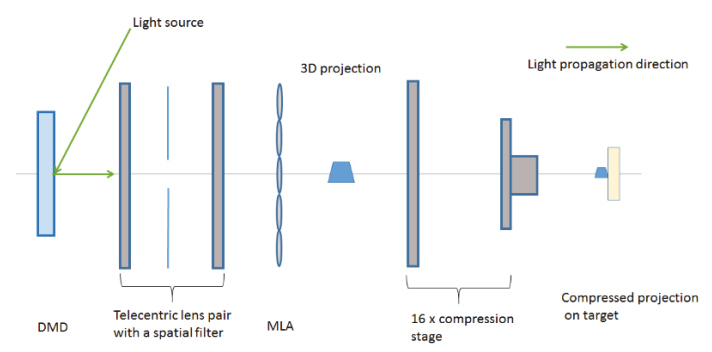


FIGURE 1: DMD BASED 3D LIGHTFIELD LITHOGRAPHY SYSTEM SHOWING THE POSITIONS OF THE 3D PROJECTIONS BEFORE AND AFTER THE OMPRESSION STAGE

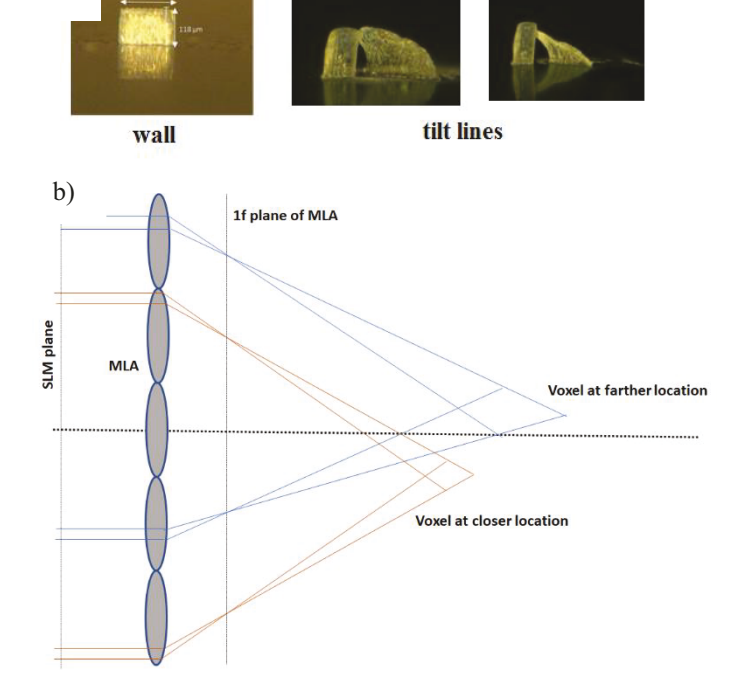


FIGURE 2: a) PATTERNS GENERATED FROM DMD BASED 3D LITHOGRAPHY SETUP. THE PATTERNS SUFFERED FROM DISTORTION. b) VOXEL SIZE VARIATION AT DIFFERENT Z POSITIONS

A phase controlled SLM usually consists of a mesh of liquid crystals (LC)[17, 18]. The alignment of LC can be changed by modifying the voltage across the pixel, which in turn changes the refractive index of the pixel. The output light beam propagation direction can be controlled by changing the voltage applied through the set of pixels in consideration. Through the use of a phase controlled SLM, we can therefore guide light beams directly to the required voxel locations. The new setup consisted of a Holoeye GAEA-2 10 Megapixel Phase Only Liquid Crystal on Silicon (LCOS)-SLM in place of the DMD - MLA

V001T16A003-2

a)

combination. The light from the SLM was transported through a telecentric lens pair with a spatial filter at the Fourier plane. The 3D image formed after the telecentric lens pair was compressed by 16 times (16 x laterally and $16^2 = 256$ x axially) and projected onto the photoresist. The modified setup is illustrated in figure 3.

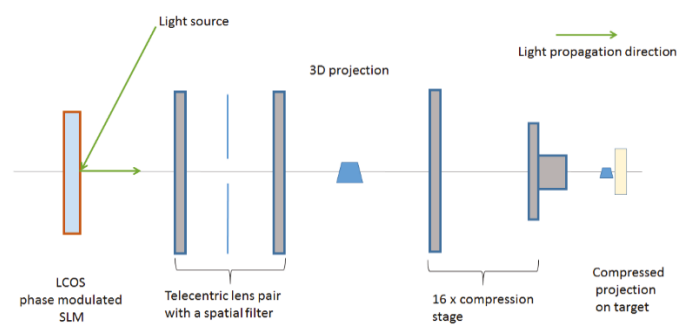


FIGURE MODIFIED LCOS SLM BASED LIGHTFIELD LITHOGRAPHY SYSTEM

2.2 3D voxel generation algorithms

The phase-controlled LCOS SLM made it possible for us to control the light beam (sub-ray) direction individually. We could create an individual voxel by focusing light at a single spot by using a Fresnel lens phase map on the SLM. The transmittance function tF(x,y) for a Fresnel lens of focal length f, for a source of wavelength λ ; and its phase function $\phi F(x,y)$ are described by the equations 1 and 2 respectively[17].

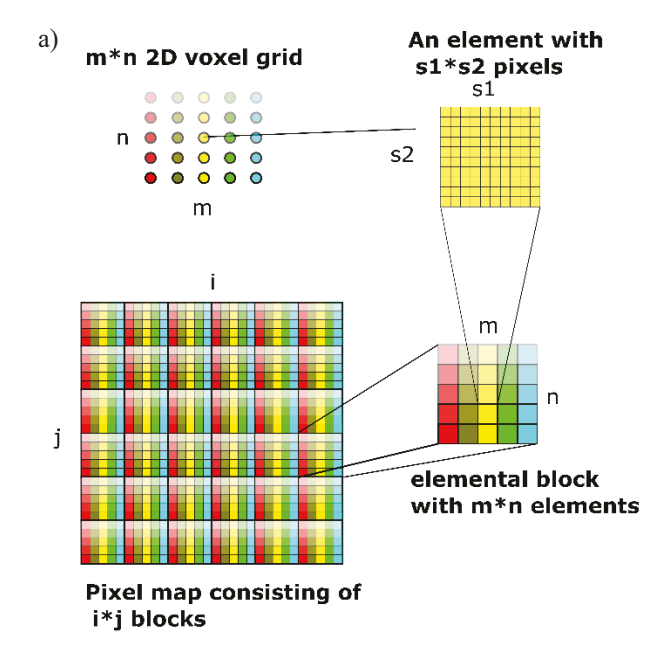
$$tF(x,y) = \exp\left[-i\frac{k}{2f}(x^2 + y^2)\right]$$
 (1)

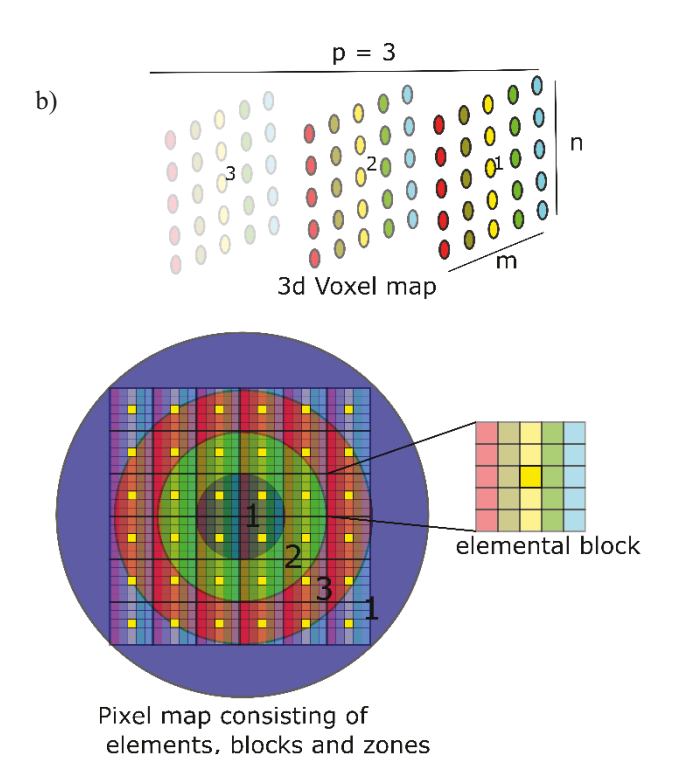
$$tF(x,y) = \exp\left[-i\frac{k}{2f}(x^2 + y^2)\right]$$

$$\phi F(x,y) = \tan^{-1}\frac{Re\{t(x,y)\}}{Im\{t(x,y)\}}$$
(2)

Where $k = \frac{2\pi}{\lambda}$ and the phase is taken to be between 0 and 2π . The Holoeye software accepts input images with pixel values between 0 and 255 to determine the voltage and consequently the phase associated with each pixel, and we scaled the phase associated with each pixel to a numeric value between 0 and 255 accordingly to create the pixel map associated with each configuration. We were able to project a single voxel at various depths by changing the f value in equation 1. By dividing the entire pixel map into a Cartesian mesh of pixels[19] we were also successful in projecting multiple voxels -a) each at the same x,y locations with different z locations, b) in a square mesh at the same z location and c) a 3D mesh of voxels at different x,y and z locations. To project a voxel array with small separation distances, phased patterns of each Fresnel lens can overlap. To handle the overlapping issue, the entire SLM pixel grid was separated into small rectangular subsections (elements). Each subsection consisted of an array of pixels depending on the separation distance of the voxels. Each of the elements was responsible for the delivery of light to a particular voxel. When the fresnel patterns of some voxels are overlapping, the common pixel elements are assigned the phase information corresponding to only one of the voxels through an algorithm described as

follows. For simplicity, let us consider an infinite pixel array to prevent the complication of dealing with the boundaries. To create an m*n grid of voxels closely sepearted at a particular z location, the entire pixel map is divided into elements of size s1*s2 where s1 and s2 are whole numbers. Each of the elements is responsible for providing illumination to a voxel. The elements can now be grouped into blocks of size m*n which is the same size as the voxel mesh size. In this block, the (x,y)th element is a light source for the (x,y)th voxel, and hence the phases of the pixels in this element are determined only by the Fresnel equation associated with the (x,y)th voxel. Each block can therefore provide m*n sub-rays to the voxel mesh – one subray each for each of the voxels. By periodically repeating the blocks all across the SLM, we can provide multiple sub-rays to each of the voxels. Even though the above explanation was for an infinitely large SLM, the only difference when we consider a real SLM is that the blocks of m*n elements can only be repeated a finite number of times in the x and y directions. By repeating the blocks i*j times, we would have a mesh of i*j*m*n elements where i and j depend on the SLM dimensions as well as the parameters s1 and s2. The (x,y) element in a block is responsible for the generation of sub-rays associated with the (x,y) voxel-This algorithm was then extended to generate m*n*p voxels in 3D space by periodically assigning each of the elements to various z depths based on the radial distance from the center of the voxel. The 2D algorithm assigns the (m,n)th element of a block to the (m,n)th voxel in the 2D mesh. If we have a 3D mesh, there would be voxels at the (m,n,z1), (m,n,z2),...(m,n,p)positions. The (m,n)th element can still only provide light subrays to one of the (m,n,z) voxels. To overcome this deficit, one solution we explored was to virtually divide the pixel maps concentrically with respect to the center of the (m,n,1) voxel. The (m,n) element in the innermost circle was programmed with the phase information of the (m,n,1) voxel. The (m,n) elements in the second annular region were then assigned to the voxel (m.n.2) and so on. These elements are illustrated in figure 4b by yellow squared and the voxels associated with each of the zones labelled 1,2,3 are indicated in the voxel map by the same labels. The voxel generation algorithm is illustrated in figure 4. The pixel maps generated for various configurations using the Fresnel lens equation (equation 1) are also shown in figure 4.





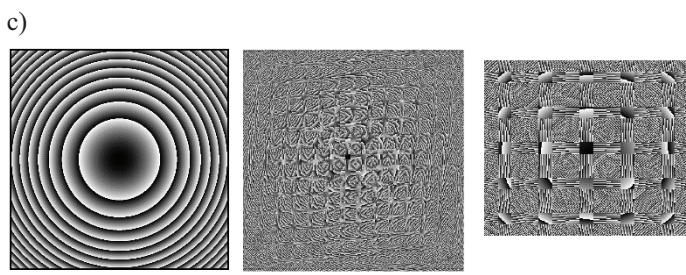


FIGURE 4: a) M*N VOXEL GRID AND ITS ASSOCIATED PIXEL MAP DIVISION. THE YELLOW SPOT IN THE MIDDLE CAN BE FORMED BY THE YELLOW ELEMENTS AT THE (2,2) POSITIONS OF EACH BLOCK. EACH BLOCK IN TURN CONSISTS OF A GRID OF PIXELS ACTING AS A LIGHT SOURCE. b) 3D VOXEL ARRAY AND THE ASSOCIATED PIXEL MAP DIVISION. THE YELLOW SPOTS AT THE 3 Z LOCATIONS INDICATED BY 1,2,3 ARE ASSOCIATED WITH THE YELLOW CONTAINED BY THE ANNULAR REGIONS LABELLED 1,2&3 RESPECTIVELY. c) FROM LEFT TO RIGHT -PIXEL MAPS FOR 1 SPOT, 2D ARRAY OF SPOTS AND ZOOMED VIEW OF THE 3D ARRAY USING FRESNAL EQUATION

The images projected from the above algorithm were able to focus the light at exactly the required voxel locations. However, Fresnel phase patterns have a very large period at the center region and a very small period around the outer perimeter. The large period around the center cannot be adequately projected when they are cropped into a lot of small separated pieces with this algorithm to accommodate the overlapping of the Fresnel lens patterns when multiple voxels are close to each other: each small cropped region acts as an aperture of propagating light. The aperture can cause strong light diffraction when the period of the light is large. On the other hand, the very small period of the diffraction pattern close to the outer perimeter of the Fresnel lens cannot be well handled with the digital phase controlled SLM with limited pixel size (~4 µm). Another issue of this algorithm of projecting light with the Fresnel lens pattern is the change of the optical length from the SLM to the focal spot, which is undesired in two-photon lithography with a femtosecond laser. Thus, we developed a second 3D projection method with Fresnel Axicon patterns via the phase-controlled SLM.

By projecting an Axicon[20, 21] pattern on the SLM, we can provide uniform intensity as well as uniform convergence angles for a large range of z depths. The transmittance function tA(x,y) for an axicone are described by the equation 3 and 4[21]

$$tA(x,y) = \exp(-i k(n-1)(x^2 + y^2)^{0.5} p \tan \theta)$$
 (3)

Where n is the refractive index of the LCOS SLM pixels, p is the pitch of the pixels and θ is angle of the axicon which can be calculated from the convergence angle of the voxel, α as

$$\theta = \sin(\alpha)(n-1) \tag{4}$$

The final projected patterns in the previous setup were designed to be around 200 micrometers high after a compression of 256 times. The patterns after the first telecentric lens are therefore constrained to a length of $\sim \! 50$ mm. The voxel resolution in the x,y and z directions are kept the same and the angle of the sub-rays are restricted to 45 degrees and the required convergence angle after the SLM come out to 3.57 degrees as illustrated in figure 5. With these constrains coupled with the Holoeye SLM specifications, the radius of the axicone annular

ring for the nearest and farthest voxels are calculated to be 90 and 900 pixels respectively. This is further explained in figure 5.

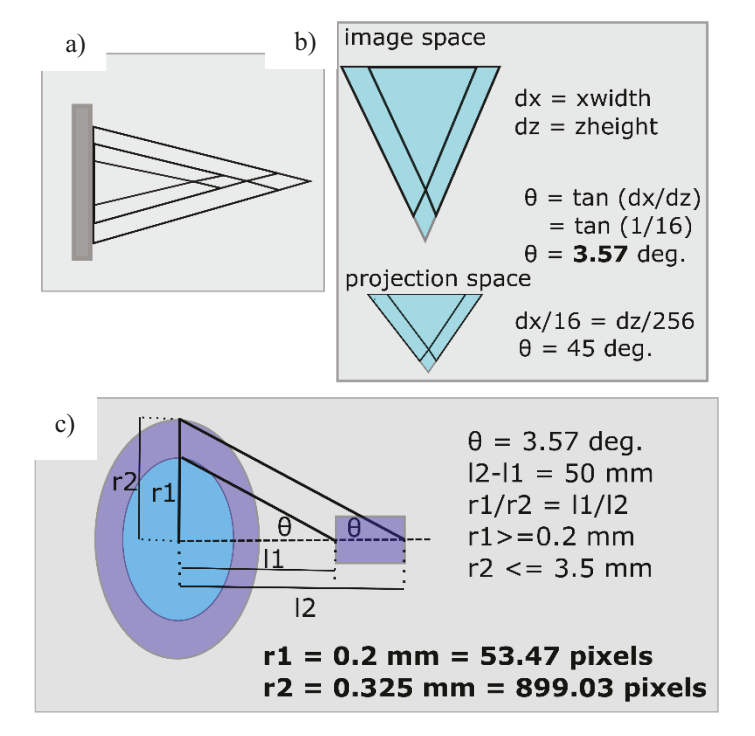


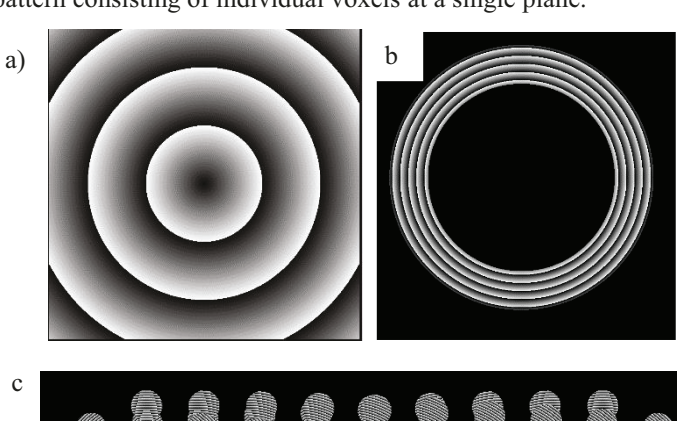
FIGURE 5: a) AXICON PROJECTIONS OF 2 VOXELS b,c) CALCULATION OF THE CONVERGENCE ANGLE OF THE RAYS AND THE AXICON PATTERN RADII RANGE FOR A 200 MICRON PROJECTION

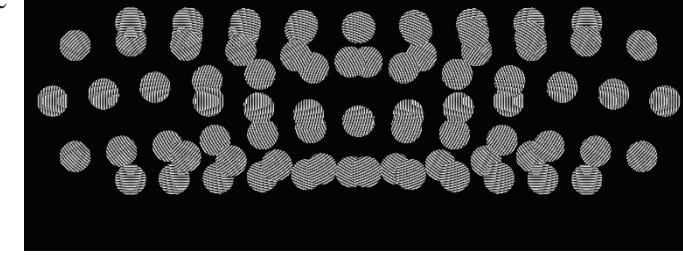
The axicon patterns on the SLM have a uniform phase period independent of the distance from the center of the voxel. This property allows the pixel elements to provide the same convergence angle at all z positions, which is essential in the projection of uniform voxels throughout the 3D space. Moreover, rays can arrive at the designed voxel locations with the same optical lengths, which is required in two-photon absorption with femtosecond light. The elemental aperture size can be controlled to a size large enough to accommodate the period of the axicon to prevent the diffraction patterns at the voxel location. The radial symmetry of the axicon patterns also makes it easier to divide the SLM into annular disks of the uniform period. This is illustrated in figure 7. Each annular disk is responsible for one voxel, but the disks farther from the center contain more pixels compared to the disks closer to the center. In order to project a 3d mesh of voxels, we have to ensure that (1). The pattern overlap for nearby voxels is prevented, and (2). Each voxel receives the same intensity of light at all z depths. By dividing the annular disks into circular elemental apertures of the same radius, we can solve both the aforementioned issues. The total number of apertures used for each voxel position can be made the same to ensure uniform intensity, and the apertures can be created at optimal positions to prevent overlapping of the light sources for multiple voxels. The size of the aperture determines

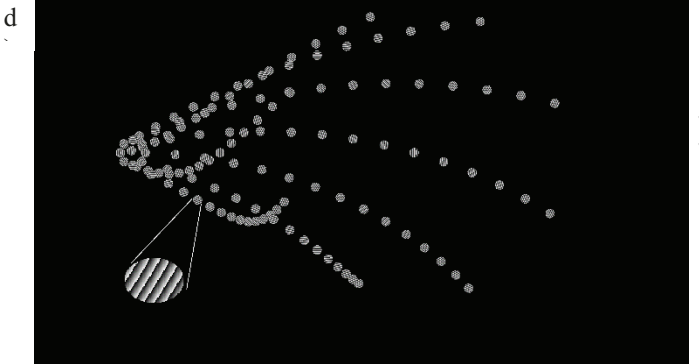
the size of the voxel, and the radial distance of the aperture determines the z position of the voxel. Because the light reflected from unused pixels of the SLM can affect the projection contrast, high period blaze grating phase patterns are assigned to these unused pixels to diffract used light beams into one specific direction. These used light beams can then be filtered out with a spatial filter to maintain high contrast of the projection patterns with the SLM.

3. RESULTS AND DISCUSSION

The discretized axicon patterns were used to project a line of voxels at the same z location to test the 2d projection using the parameters calculated in the previous section. The background light from the unused pixels was blocked by the spatial filter to project a high contrast image of the linear voxel mesh. The pattern was then modified to project the voxels at different z depths to obtain a 3D pattern and the projection results were captured onto a screen. The pixel maps and the projected images are shown in figure 6. We can clearly see the sharp linear pattern consisting of individual voxels at a single plane.









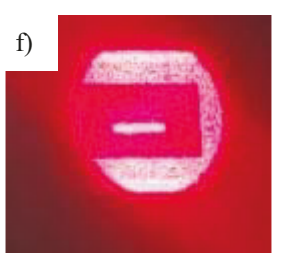


FIGURE 6: a) FROM LEFT TO RIGHT TOP TO BOTTOM a) COMMPLETE AXICON PIXEL MAP b) ANNULAR AXICON PATTERN TO ILLUMINTE 1 VOXEL c) DISCRETIZED AXICON PATTERNS FOR A STRAIGHT LINE d) DISCRETIZED AXICON PATTERN FOR A TILT LINE WITH THE CIRCULAR APERTURE ZOOMED IN THE INSET. WE CAN NOTICE THE UNIFORM PERIOD IN ALL THE PATTERNS. THE STRAIGHT LINE PATTERN HAS AXICONS OF THE SAME RADII AS ALL THE VOXELS ARE IN THE SAME PLANE WHEREAS THE TILTED LINE WHICH SPANS OVER MULTIPLE Z DEPTHS HAS AXICON OF VARYING RADII e,f) CAPTURED IMAGES OF THE STRAIGHT LINE WITH AND WITHOUT THE SPATIAL FILER RESPECTIVELY. THE SPATIAL FILTER BLOCKS THE BACKGROUND REFLECTED LIGHT FROM THE SLM AND ONLY ALLOWS THE LIGHT SENT BY THE **AXICON APERTURES**

The pixel maps for the dense line and tilt line patterns are slightly overlapped but this can be reduced even further by selecting the appropriate voxel separation distance and the angular separation of the pixel aperture elements. We can extend the pixel maps for more complex 3D structures as well based on the algorithm described in this study with the added benefit of having uniformly sized and illuminated voxels at all z locations within the range permitted by the system (20 microns).

4. CONCLUSION

By using phase controlled SLM, we were able to manipulate millions of sub-rays propagating along with the designed directions with minimum divergence. By using these quasi-collimated sub-rays, we are able to generate 3D voxel clouds with continuous and femtosecond lights. Two different algorithms based on Fresnel lens and Fresnel Axicon phase functions are developed for generated 3D voxel clouds at design location as 3D volumetric projection. Compared with the Fresnel lens algorithm, the Fresnel Axicon algorithm can generate voxels with consistent size and shape for all 3D locations. Also, sub-rays can arrive at designed voxels locations with the same optical length by using the Fresnel Axicon phase function algorithm, which is required in femtosecond twophoton lithography based on the 3D volumetric projection. We will demonstrate femtosecond two-photon lithography with the 3D volumetric projection using the Fresnel Axion algorithm in the near future.

ACKNOWLEDGEMENTS

The research is support by the National Science Foundation (CMMI-1826078). The authors like to appreciate technical

supports from Dr. Yakovlev's group at TAMU.

REFERENCES

- [1] Hassanin, H., Sheikholeslami, G., Sareh, P., and Ishaq, R. B., 2021, "Microadditive Manufacturing Technologies of 3D Microelectromechanical Systems," Adv Eng Mater, p. 2100422.
- [2] Wang, C., Taherabadi, L., Jia, G., Kassegne, S., Zoval, J. V., and Madou, M. J., "Carbon-MEMS architectures for 3D microbatteries," Proc. MEMS, MOEMS, and Micromachining, International Society for Optics and Photonics, pp. 295-302.
- [3] Bartolo, P., Domingos, M., Gloria, A., and Ciurana, J., 2011, "BioCell Printing: Integrated automated assembly system for tissue engineering constructs," CIRP annals, 60(1), pp. 271-274.
- [4] Domingos, M., Intranuovo, F., Russo, T., De Santis, R., Gloria, A., Ambrosio, L., Ciurana, J., and Bartolo, P., 2013, "The first systematic analysis of 3D rapid prototyped poly (ε-caprolactone) scaffolds manufactured through BioCell printing: the effect of pore size and geometry on compressive mechanical behaviour and in vitro hMSC viability," Biofabrication, 5(4), p. 045004.
- [5] Guan, Z., Jia, S., Zhu, Z., Zhang, M., and Yang, C. J., 2014, "Facile and rapid generation of large-scale microcollagen gel array for long-term single-cell 3D culture and cell proliferation heterogeneity analysis," Analytical chemistry, 86(5), pp. 2789-2797.
- [6] Urrios, A., Parra-Cabrera, C., Bhattacharjee, N., Gonzalez-Suarez, A. M., Rigat-Brugarolas, L. G., Nallapatti, U., Samitier, J., DeForest, C. A., Posas, F., and Garcia-Cordero, J. L., 2016, "3D-printing of transparent bio-microfluidic devices in PEG-DA," Lab on a Chip, 16(12), pp. 2287-2294.
- [7] Prado-Prone, G., Bazzar, M., Focarete, M. L., García-Macedo, J. A., Perez-Orive, J., Ibarra, C., Velasquillo, C., and Silva-Bermudez, P., 2020, "Single-step, acid-based fabrication of homogeneous gelatin-polycaprolactone fibrillar scaffolds intended for skin tissue engineering," Biomed Mater, 15(3), p. 035001.
- [8] Stampfl, J., Baudis, S., Heller, C., Liska, R., Neumeister, A., Kling, R., Ostendorf, A., and Spitzbart, M., 2008, "Photopolymers with tunable mechanical properties processed by laser-based high-resolution stereolithography," Journal of Micromechanics and Microengineering, 18(12), p. 125014.
- [9] Creff, J., Courson, R., Mangeat, T., Foncy, J., Souleille, S., Thibault, C., Besson, A., and Malaquin, L., 2019, "Fabrication of 3D scaffolds reproducing intestinal epithelium topography by high-resolution 3D stereolithography," Biomaterials, 221, p. 119404.
- [10] Shaw, L. A., Chizari, S., Shusteff, M., Naghsh-Nilchi, H., Di Carlo, D., and Hopkins, J. B., 2018, "Scanning two-photon continuous flow lithography for synthesis of high-resolution 3D microparticles," Optics express, 26(10), pp. 13543-13548.

- [11] Miwa, M., Juodkazis, S., Kawakami, T., Matsuo, S., and Misawa, H., 2001, "Femtosecond two-photon stereo-lithography," Applied Physics A, 73(5), pp. 561-566.
- [12] Ross, I., Davis, G., and Klemitz, D., 1988, "High-resolution holographic image projection at visible and ultraviolet wavelengths," Appl Optics, 27(5), pp. 967-972.
- [13] Shusteff, M., Panas, R. M., Henriksson, J., Kelly, B. E., and Browar, A. E., "Additive fabrication of 3d structures by holographic lithography," Proc. 2016 International Solid Freeform Fabrication Symposium, University of Texas at Austin
- [14] Zhang, H., and Wen, S. B., 2020, "3D photolithography through light field projections," Appl Opt, 59(27), pp. 8071-8076
- [15] Zhang, H., and Wen, S.-B., "Microlens array based three-dimensional light field projection and possible applications in photolithography," Proc. Optifab 2019, International Society for Optics and Photonics, p. 111751P.
- [16] Jakkinapalli, A., Baskar, B., and Wen, S.-B., "Femtosecond Two-Photon 3D Lightfield Lithography," Proc. Heat Transfer Summer Conference, American Society of Mechanical Engineers, p. V001T013A001.
- [17] Rosales-Guzmán, C., and Forbes, A., 2017, How to shape light with spatial light modulators, SPIE Press.
- [18] Zhang, Z., You, Z., and Chu, D., 2014, "Fundamentals of phase-only liquid crystal on silicon (LCOS) devices," Light: Science & Applications, 3(10), pp. e213-e213.
- [19] Romero, L. A., Millán, M. S., and Pérez-Cabré, E., "Optical implementation of multifocal programmable lens with single and multiple axes," Proc. Journal of Physics: Conference Series, IOP Publishing, p. 012050.
- [20] Golub, I., 2006, "Fresnel axicon," Optics letters, 31(12), pp. 1890-1892.
- [21] Zhai, Z., Cheng, Z., Lv, Q., and Wang, X., 2020, "Tunable Axicons Generated by Spatial Light Modulator with High-Level Phase Computer-Generated Holograms," Applied Sciences, 10(15), p. 5127.